COMPUTATIONAL MODELING OF MICRO-CRACK INDUCED ATTENUATION IN CFRP COMPOSITES

R.A. Roberts[1] and C.A.C. Leckey[2]
[1]Center for NDE, Iowa State University, Ames, IA 50014
[2]NASA Langley, Hampton, VA 23681

ABSTRACT. A computational study is performed to determine the contribution to ultrasound attenuation in carbon fiber reinforced polymer composite laminates of linear elastic scattering by matrix micro-cracking. Multiple scattering approximations are benchmarked against exact computational approaches. Results support linear scattering as the source of observed increased attenuation in the presence of micro-cracking.

Keywords: Ultrasound, Composites, Micro-crack
PACS: 43.35.Yb 43.35.Zc 43.38.Hz

INTRODUCTION

This paper reports on work to nondestructively detect damage in carbon fiber reinforced polymer composites (CFRP) at the earliest possible stage of damage evolution. Damage in CFRP material systems can initiate as small distributed micro-cracks in the polymer matrix, introduced through, say, an accidental impact, which then grow and coalesce through cyclic loading into large-scale ply delamination, ultimately leading to structural failure. An established tool for detection of large-scale ply delamination is pulse-echo ultrasound, which looks for a strong reflection from the separated ply interfaces.[1] In addition to the detection of large-scale ply delamination, NASA is interested in detecting the presence of ply micro-cracks prior to advancement to delamination. It was hypothesized by NASA, supported by experimental evidence, that monitoring ultrasound attenuation in the CFRP structure might be a means to detect the presence of micro-cracks. To examine this hypothesis, a computational study of the interaction of ultrasound with distributed micro-cracking in a composite laminate was undertaken, the results of which are presented here. The purpose of the computational study is to provide predictions of ultrasound attenuation as a function of micro-crack volumetric density, which in subsequent work could be correlated with experimental observations made in well characterized specimens.

Experimental evidence of micro-crack induced attenuation has been observed by NASA. CFRP composite laminate specimens were prepared into which micro-cracking was introduced through thermal and mechanical cycling. X-ray CT data were collected on the specimens that verified the presence of pre-delamination micro-cracking. A specimen was selected for ultrasonic examination which the CT data revealed to have an increasing volume density of micro cracks with distance along the specimen. Ultrasound attenuation was observed by recording back-wall reflections as a function of position, using a 5 MHz mildly focused transducer focused on the back-wall. A back-wall reflection C-scan image is shown in fig.(1). The specimen is a 16 ply $[45/90/-45/0]_{2S}$ quasi-isotropic

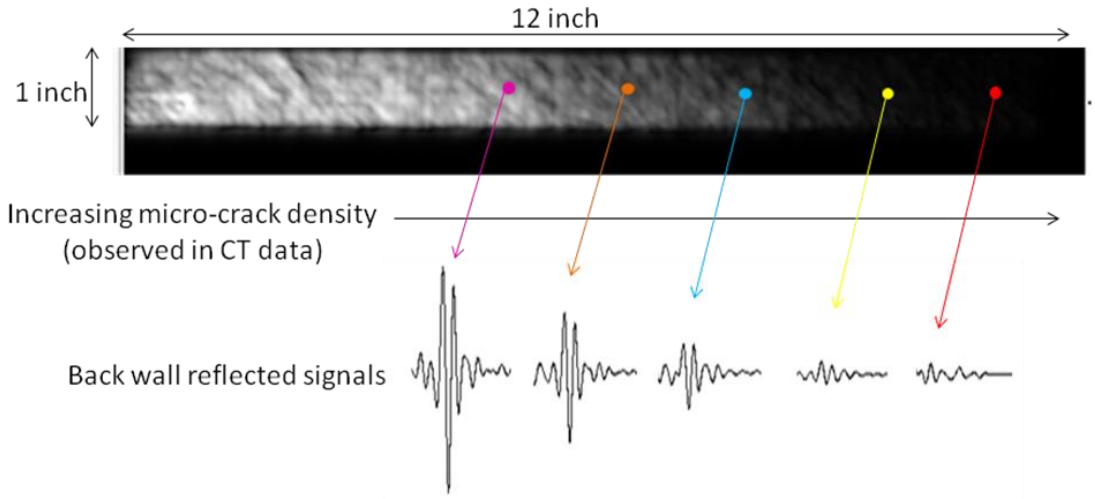

FIGURE 1. Experimental observation of micro-crack induced attenuation.

laminate with dimensions 12 inches by 1 inch. Decreasing signal amplitude is evident with distance along the length of the specimen, corresponding to the increasing micro-crack density observed in the associated CT data. Recorded A-scan signals are shown at five positions along the length of the specimen showing the decrease in signal amplitude.

Motivated by experimental observations such as shown in fig.(1), a computational study was undertaken to establish the plausibility of the observed attenuation being attributable to linear elastic wave scattering by distributed micro-cracking. Modeling efforts at CNDE employed a boundary integral equation (BIE) problem formulation facilitating analytical approximation. A parallel activity was pursued at NASA Langley which applied a finite difference based computational method to the governing elastodynamic partial differential field equations. Predictions of ultrasound attenuation were obtained as a function of volumetric micro-crack density. Results of the two computational approaches were compared, and the validity limits of approximate multiple scattering theories were observed. Overall, the study lends plausibility to the attenuation observed in fig.(1) being attributable to linear wave scattering.

NUMERICAL METHODS AND PROCEDURES

CFRP laminates of non-woven polymer impregnated tape are considered in which the reinforcing fiber orientation in successive plies can be uniformly oriented (unidirectional laminate), or vary in a specified ply-to-ply angular pattern (quasi-isotropic laminate). The individual plies are mechanically modeled as homogeneous linearly elastic continua displaying transverse isotropy with symmetry about the reinforcing fiber direction. As such, mechanical properties are specified by mass density ρ and five independent elastic constants, with stress τ_{ij} and displacements u_i related via the constitutive relation $\tau_{ij}=c_{ijkl}\ u_{k,l}$. Wave motion within the laminate is governed by the elastodynamic field equation, expressed in partial differential equation (PDE) form as

$$c_{ijkl}\, u_{k,lj}(x) - \rho\, \ddot{u}_i(x) = 0 \qquad (1)$$

with continuity of displacements and tractions at the ply interfaces imposed as boundary conditions.[2] Work presented here obtains solutions to eq.(1) using two substantially different approaches. Work at NASA applies the Elastodynamic Finite Integration Technique (EFIT), which operates directly upon eq.(1) using finite difference

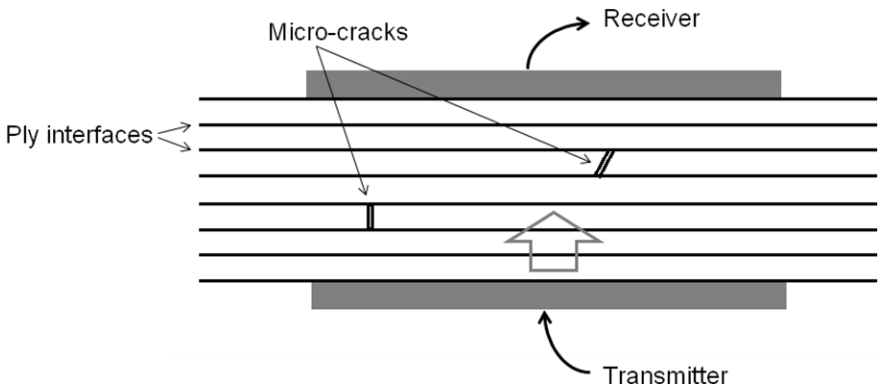

FIGURE 2. Configuration of computational model.

representations of the displacement derivatives. A detailed discussion of EFIT application to eq.(1) is found in [3] within these proceedings. Work at CNDE reformulates eq.(1) using temporal Fourier transformation and application of elastodynamic reciprocity theory to obtain an equivalent time harmonic governing boundary integral equation (BIE) defined over the traction free micro-crack surfaces C as

$$\int_C u_i(x)\, \tau^G_{ij:k}(x \mid x')\, n_j(x)\, dx + \tfrac{1}{2} u_k(x') = u^{inc}_k(x') \qquad (2)$$

where $\tau^G_{ij:k}(x|x')\, n_j(x)$ is the surface traction in response to a point load acting at position x' within a corresponding crack-free composite laminate (Green state), and $u_k^{inc}(x')$ is the incident displacement field which would exist in the crack-free laminate.[4] Solutions to eq.(2) are obtained through application of the Boundary Element Method (BEM), which transforms the BIE into a matrix equation by expressing the displacements $u_i(x)$ as a weighted sum of appropriate basis functions, the solution of which yields the weighting coefficients. A detailed discussion of the BEM methods used to solve eq.(2) is presented in [5] in these proceedings.

Ultrasonic attenuation is perceived as a reduction in receiver output voltage, as exemplified in fig.(1). Model predictions of receiver output voltage are obtained through application of Auld's reciprocity relation, which relates generated and detected wave fields to input and output transducer voltages. Specifically, Auld's relation expresses the change in receiver output voltage δv due to introduction of a wave field on a surface S having normal n_j, arising from a transmitting transducer, expressed here as

$$\delta v = \Gamma \int_S (\dot{u}_i^A(x)\, \tau_{ij}^B(x) - \dot{u}_i^B(x)\, \tau_{ij}^A(x))\, n_j(x)\, dx \qquad (3)$$

where "A" indicates the field introduced over surface S, and "B" indicates the field which would exist at the location of S were the receiver used reciprocally as a transmitter. The factor Γ represents among, other things, the electro-mechanical conversion efficiency of the transducers.[6]

The problem configuration considered is depicted in fig.(2). A transmitter and receiver are positioned on opposing sides of a composite laminate, containing some number of micro-cracks. Longitudinal motion transducers are assumed, i.e., were the transducers infinite in extent, they would generate a longitudinal plane wave emerging perpendicular to the transducer face. When considering finite dimensions, the transducers additionally generate and receive edge diffracted signals. The dimension of the receiving transducer is prescribed to cover the reference volume of composite material into which micro-cracks are distributed. The transmitter is assumed to be as large as (or larger than) the receiver. Computations using EFIT prescribe a 3D computational grid to a selected volume between the transmitter and receiver, typically larger than the reference volume of

interest by an appropriate margin to reduce the influence of reflections from the sides of the computational grid. The computation obtains the evolution in time of fields within the laminate arising in response to a prescribed pulse of mechanical loading on the transmitter surface. The receiver output voltage is obtained by applying eq.(3) over the laminate surface in contact with the face of the receiver, where field "A" is the transmitted field reaching the receiver surface after interacting with any present micro-cracks, and field "B" is a segment of a downward propagating longitudinal plane wave limited in extent to the receiver dimensions. The evaluation of eq.(3) predicts the receiver voltage obtained in response to the arrival of the transmitted pulse.

Application of the BIE/BEM analysis assumes a slight modification to the configuration of fig.(2). It is assumed that the composite laminate depicted in fig.(2) is infinite in extent, and is sandwiched between two half-spaces of unidirectional composite, where the material orientation of the neighboring half-spaces is assumed to match that of the adjacent laminate surface plies. The incident field and receiver fields are assumed to be plane waves of longitudinal motion propagating perpendicular to the ply interfaces, and in opposite directions. The incident wave is prescribed to have a broadband pulse temporal response. Computed time harmonic responses are therefore Fourier transformed to obtain desired temporal responses. The BIE analysis is limited to a 2D field dependency, which allows rigorous treatment of arbitrary distributions of cracks in unidirectional laminates, and uniformly aligned distributions of cracks in quasi-isotropic laminates. For determination of the crack-free transmitted voltage, eq.(3) is applied to the finite receiver surface, as described above for the EFIT calculation. In calculating the scattered signal contribution to the crack-attenuated receiver output, eq.(3) is applied in a somewhat different fashion. Rather than integrating over the receiver face, field "B" in eq.(3) is taken as the field on the surface of the micro-cracks. Noting the traction-free condition of the crack surfaces, eq.(3) becomes

$$\delta v = \Gamma \int_C \dot{u}_i(x)\, \tau_{ij}^{rec}(x)\, n_j(x)\, dx \tag{4}$$

where C indicates the surface of the micro-crack(s). Although the receiver is prescribed to have a finite extent, it is noted that the receiver field on the crack surfaces can be effectively approximated as an infinite plane wave in the evaluation of eq.(4).[5]

Employing Auld's relation in the form of eq.(4) leads to useful analytic approximations of the micro-crack induced attenuation. Fields on the crack surfaces are obtained as BEM solutions to eq.(2). The BIE formulation enables derivation of approximate multiple scattering models, in which the interaction of scattered fields between neighboring cracks are treated in a sequential fashion. Specifically, letting the level 0 contribution be the received signal in the absence of any cracks, the level 1 contribution is that resulting from interaction of the incident field with the cracks, in which contributions to the output signal are individually summed as if no other cracks were present. The level 2 contribution is that resulting from the level 1 scattered fields interacting with neighboring cracks, and so on for levels 3, 4, and higher. It is shown in [5] that such an analysis represents an iterative BIE solution, for which convergence may or may not occur, depending on crack density. Under the restriction of 2D field dependence, multiple scattering contributions of all levels are obtainable for unidirectional laminates, and quasi-isotropic laminates with aligned crack distributions. For non-aligned cracks in quasi-isotropic laminates, the level 1 contribution is readily obtained, and level 2 contributions can be approximated through an asymptotic analysis.

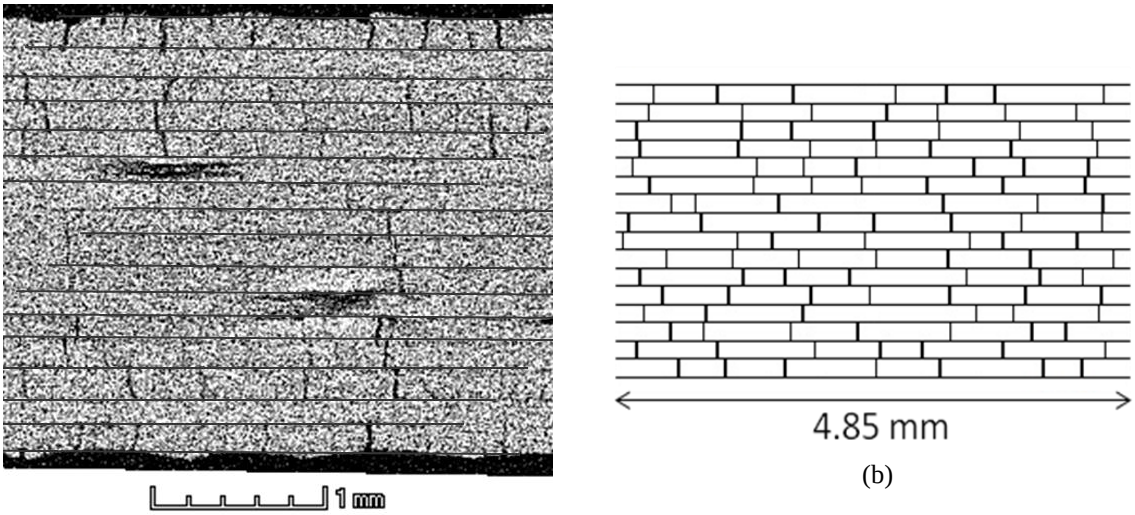

FIGURE 3. a) Micrograph of matrix micro-cracks, b) random crack distribution for computational model.

NUMERICAL RESULTS

Numerical results are presented for the case of a 16 ply composite laminate containing distributed micro-cracks. Elastic constants of the transversely isotropic plies are prescribed, using Voigt notation, as C_{11}=12.3, C_{12}=6.25, C_{13}=5.94, C_{33}=175.0, C_{44}=5.29, in GPa units, where a local ply coordinate system is assumed to have x_3 as the material symmetry axis, and density is assigned ρ=1.57E3 kg/m^3. A ply thickness of 0.16mm is prescribed. Results are shown for a unidirectional laminate, and a $[0/90]_{4s}$ cross-ply laminates.

The specification of the micro-crack distribution in the laminate was guided by micrographic examination of actual matrix micro-cracking. An example is presented in fig.(3a) showing micro-cracking in a 16 ply quasi-isotropic laminates with 0.16mm thick plies. The ply boundaries are highlighted by horizontal lines. Micro-cracks are seen to be distributed through the plies, with spacing ranging roughly from 0.2mm to 1mm apart, corresponding to a crack density of ~100 cracks/cm, where crack density is parameterized by summing over all plies the number of cracks in each ply per unit length parallel to the ply interface, and perpendicular to the fiber direction. The elongated indications in the 6th ply from top and bottom represent micro-cracks in plies having fibers oriented nearly parallel to the plane of the micrograph.

Using fig.(3a) as a guide, an algorithm for randomly distributing micro-cracks throughout the laminate was devised. A rectangular volume of the laminate was selected for study, having surface dimensions of 4.85mm x 4.85mm. The algorithm takes as input the desired number of cracks per ply within this volume, divides the extent of the ply perpendicular to the fiber direction into a corresponding number of cells, then generates the position of a crack within each cell using a random number generator. This approach was taken to assure that the assigned crack positions are distributed across the volume, as observed in fig.(3a), rather than all possibly being clumped near one location, as was seen to occur if the location is not restricted to a corresponding cell. For the calculations presented here, it is assumed that the micro-cracks are all oriented perpendicular to the ply interfaces, are effectively infinite in extent in the fiber direction, and have a crack opening equal to 5% of the crack height (.008 mm). A crack distribution generated in this fashion is shown in fig.(3b) for a unidirectional composite. The distribution has 112 cracks within a 4.85mm wide test volume, representing a crack density of 230 cracks/cm.

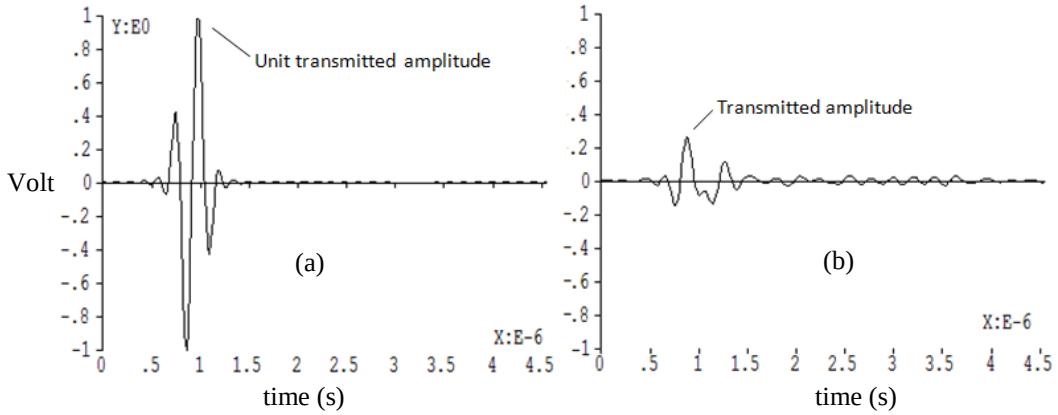

FIGURE 4. Transmitted time signals: a) no cracks, b) crack density = 230 cracks/cm.

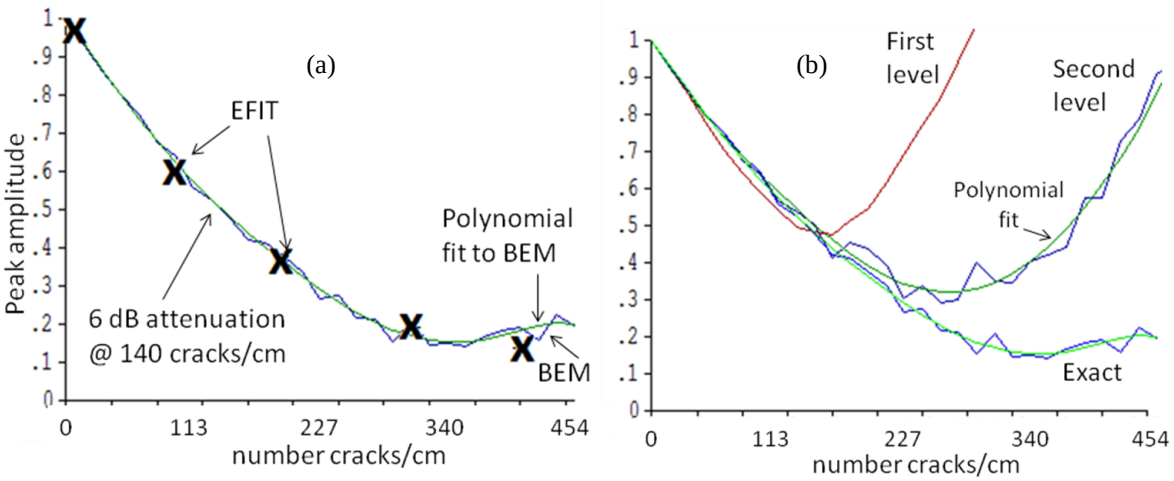

FIGURE 5. a) Peak signal versus crack density, b) comparison of multiple scattering theories

Results are first presented for a unidirectional composite. A 4.85 mm x 4.85 mm volume of interest is selected, with corresponding receiver dimensions. The temporal response of the incident displacement is assumed to have a Hanning window frequency spectrum with 100% bandwidth and a 3.5 MHz center frequency. Receiver output signals obtained using the BIE/BEM computation are shown in fig.(4) for the case of a) no micro-cracks, and b) 112 cracks within the test volume, corresponding to fig.(3b). The BEM computation in fig.(4b) explicitly includes all crack surfaces in a single, large BEM matrix, and as such fully accounts for all multiple crack interactions. In this regard it is referred to as an exact solution. The reduction in signal amplitude seen in fig.(4b) is attributed to micro-crack scattering attenuation.

Computations similar to fig.(4) were carried out for random crack distributions having densities ranging from 0 to 460 cracks/cm, (0 to 224 cracks within the test volume, in 8 crack increments). Exact scattering results were obtaining using the fully-interacting BEM matrix. Additionally, EFIT predictions of transmitted peak signal amplitudes were computed for crack distributions having 8, 48, 96, 152, and 200 cracks within the test volume. Results of both the BEM and EFIT computations are plotted in fig.(5a), which display good agreement. It is noted that a degree of random noise is observed in the plot of peak signal amplitude, resulting from the random nature of the crack configuration. For this reason, a polynomial fit to BEM data is also plotted in fig.(5a), representing the anticipated mean of the random fluctuation.

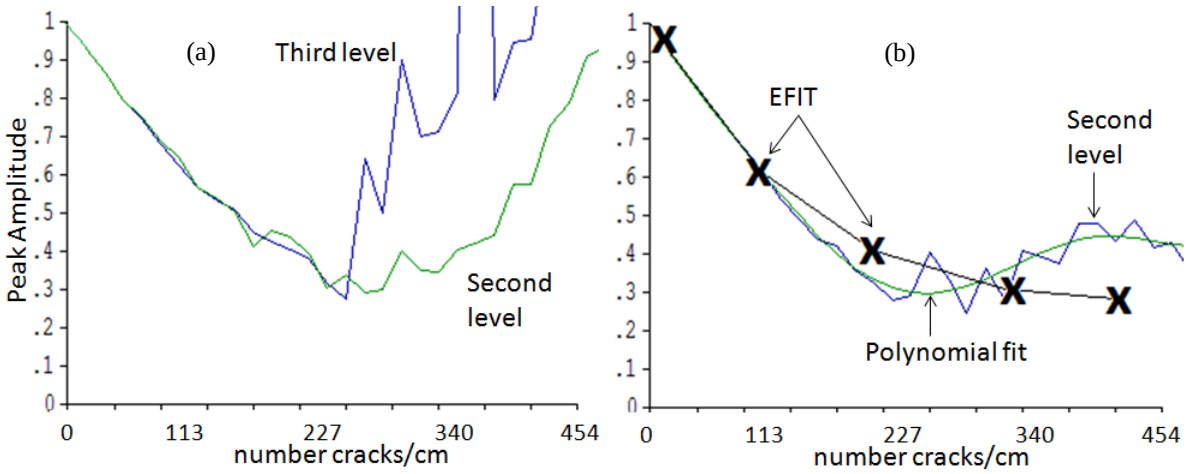

FIGURE 6. a) Comparison of 2nd and 3rd level multiple scattering, b) 2nd level result in cross-ply laminate.

The validity of approximate multiple scattering theory is examined by computing the contributions of sequential levels of scattering interactions, as described in the preceding section. The 0th level interaction is the crack-free transmitted field of fig.(4a). The contribution of the first level interaction (independent scattering approximation) and second level interaction (scattering of the first level scattered fields) are readily computed using a BEM matrix for a single crack, as discussed in [5]. Fig.(5b) compares first and second level scattering contributions to the exact result. Again, polynomial fits are provided to indicate the expected mean of the anticipated random amplitude fluctuation. It is seen that the three predictions are in agreement for crack densities less than ~150 cracks/cm. Above this value, both approximations display divergent behavior, with the second level scattering contribution presenting less error than the first level contribution. The result of fig.(5b) provides an indication of the useful range of approximate multiple scattering theory. For example, should it be determined that micro-crack densities less than 150 cracks/cm are of primary interest, first level approximation (independent scattering theory) would prove adequate.

It is significant to note that increasing the level of scatter interaction does not assure improvement in the result: as with all diverging series, adding more terms to a diverging series need not improve the result. This is demonstrated in fig.(6a), which compares second and third level scattering contributions as a function of crack density. It is observed that for crack densities less than 240 cracks/cm, the third level contribution improves the approximation, bringing it in close agreement with the exact result. However, for crack densities greater than 240 cracks/cm, the additional level of scattering interaction significantly worsens agreement with the exact result, consistent with the divergence of the series.

Application of the modeling approaches to a cross-ply laminate will now be discussed. As the EFIT calculation performs a full 3D field calculation, application to the cross-ply geometry is straightforward and unimpeded. In contrast, the BEM analysis employed here assumes a 2D dependence of the field on spatial position, and therefore cannot be used for exact computation of multiple scattering interactions in the general cross-ply micro-crack configuration, where cracks are not uniformly oriented. Rather, the BEM analysis can be used to compute only first and second level scattering interactions. Results are presented here comparing the BEM 2nd level scattering prediction with the EFIT prediction for a 16 layer cross-ply laminate having alternating 0 and 90 degree ply

orientations. Ply thickness and mechanical properties are the same as those for the unidirectional laminate. As before, level 2 BEM scattering predictions of attenuation were obtained for 0 to 224 cracks in the test volume in 8 crack increments (0 to 460 cracks/cm), and corresponding EFIT results were obtained for 8, 48, 96, 152, and 200 cracks within the test volume. The predictions are compared in fig.(6b). As in the unidirectional composite, the approximate model provides an effective prediction for low crack densities. However, unlike the unidirectional case, the approximate model is seen to over-predict the attenuation at higher crack densities. This behavior is suspected to arise from the nature of approximation made in deriving this result, and will receive more detailed study in the future. Nonetheless, the approximation is observed to provide a useful prediction of attenuation over a substantial range of the crack densities examined.

Computer run times varied substantially with the level of problem approximation. To give an indication, the first level scattering approximation requires a fraction of a second running on a laptop PC, whereas an explicit BEM matrix inversion for scattering by 100 cracks requires 20 minutes. In contrast, the 3D EFIT calculation requires 20 hours on a 128 core PC cluster.

SUMMARY AND CONCLUSIONS

It is concluded from this study that linear elastic scattering is a plausible cause of increased ultrasound attenuation observed in the presence of matrix micro-cracking CFRP composites. This enables the use of a linear scattering model to quantitatively relate observed attenuation to micro-crack density, leading to a quantitative measure of early damage in composites. It is established that an independent scattering assumption adequately predicts micro-crack induced attenuation at sufficiently low crack densities (< ~100 cracks/cm in the cases examined). Higher order scatter assumptions yield improved predictions over marginally increased ranges of crack density. Computations were benchmarked as consistent using substantially different computational methods, lending credibility to the reported observations. Model predictions agree qualitatively with experimentally observed behaviors, and future work to quantify specimen crack densities will enable quantitative comparisons.

ACKNOWLEDGEMENT

This work is supported by NASA under award NAG-1-029098.

REFERENCES

1. F. Margetan, C.A.C. Leckey, D. Barnard, “Modeling the Effects Of Beam Size and Flaw Morphology on Ultrasonic Pulse-Echo Sizing of Delaminations in Carbon Composites,” *these Proceedings*.
2. J. Achenbach, *Wave Propagation in Elastic Solids*, Elsevier, 1982.
3. C.A.C. Leckey, M.D. Rogge and F.R. Parker, ”Microcracking In Composite Laminates: Simulation Of Crack-Induced Ultrasound Attenuation,” *these proceedings.*
4. J. Achenbach, *Reciprocity In Elastodynamics*, Cambridge, UK, 2003.
5. R. Roberts, “Micro-Crack Ultrasound Scattering In Anisotropic Composite Laminates”, *these proceedings.*
6. B. Auld, “General Electromechanical Reciprocity Relations Applied to the Calculation of Elastic Wave Scattering Coefficients,” Wave Motion Vol. 1, 1979.